Composites: Part A 56 (2014) 192–202

Contents lists available at ScienceDirect

Composites: Part A

journal homepage: www.elsevier.com/locate/compositesa

Strength prediction in CFRP woven laminate bolted double-lap joints under quasi-static loading using XFEM

H. Ahmad [a,*], A.D. Crocombe [b], P.A. Smith [b]

[a] Department of Structures and Materials Engineering, Faculty of Civil and Environmental Engineering, Universiti Tun Hussein Onn Malaysia, 86400 Parit Raja, Batu Pahat, Johor Darul Tak'zim, Malaysia
[b] Department of Mechanical Engineering Sciences, Faculty of Engineering and Physical Sciences, University of Surrey, Guildford, Surrey GU2 7XH, United Kingdom

ARTICLE INFO

Article history:
Received 1 May 2013
Received in revised form 1 October 2013
Accepted 14 October 2013
Available online 22 October 2013

Keywords:
A. Textiles
B. Fracture
C. Finite element analysis (FEA)
E. Joints

ABSTRACT

The current paper is concerned with modelling damage and fracture in woven fabric composite double-lap bolted joints that fail by net-tension. A 3-D finite element model is used, which incorporates bolt clamp-up, to model a range of CFRP bolted joints, which were also tested experimentally. The effects of laminate lay-up, joint geometry, hole size and bolt clamp-up torque were considered. An Extended Finite Element (XFEM) approach is used to simulate damage growth, with traction–separation parameters that are based on previously reported, independent experimental measurements for the strength and toughness of the woven fabric materials under investigation. Good agreement between the predicted and measured bearing stress at failure was obtained.

1. Introduction

Mechanically fastened joints are used widely in composite structures. In comparison with bonded joints, there are no surface preparation issues for bolted joints, there is the option of disassembly for routine inspection and they are relatively insensitive to environmental conditions. The major challenge with mechanically fastened joints is that the introduction of a hole into a composite plate leads to a stress concentration, which cannot be relieved by plastic flow in the way that is possible in a metallic material. Hence there is a significant reduction in strength as a result of the stress concentration introduced by any hole or cut-out. Moreover the way in which damage develops in a composite in the presence of a stress-raiser is complex and currently there is a lack of design tools to enable engineers to predict reliably the strength of either open-hole or mechanically fastened composites. The present work is concerned with developing a strength prediction methodology for composite bolted joints.

Experimental studies by previous researchers mostly consider the bearing strength and associated failure modes in single-bolted connections. A vast body of work exists, addressing the effect of varying joint geometry (such as laminate thickness, hole diameter, and width/hole diameter (W/d) and end length/hole diameter (e/d) ratios) in different material types and lay-ups. In particular many studies have looked at the transition from net-tension failure to bearing failure with increasing normalised joint width, W/d, or the transition from shear-out to bearing failure with increasing normalised joint end distance, e/d. Early work by Collings [1] quantified these effects for a range of CFRP laminates and showed in particular that bearing strength and the associated mechanism of failure are strongly dependent on lay-up. Moreover larger holes undergo less stress concentration relief prior to failure, which relates to reduced strength for larger holes (the hole size effect, for which there is much work in the literature for open holes). Other early work (as reported for instance in the review by Godwin and Matthews [2]) emphasised the role of bolt clamp-up on joint strength and failure mode. Clamp-up increases the load transfer by friction and further enhances the failure strength in the bearing mode as premature failure by splitting is restricted. A recent review by Thoppul et al. [3] comprehensively investigate the mechanics of mechanically fastened joints in polymer–matrix composite structures, including joint design methodologies and the selection of fastener pre-load.

With regard to stress analysis and strength prediction for composite bolted joints, there are some relatively simple analytical approaches in the literature, which for the most part treat the problem as two-dimensional. In reality, the effects of finite joint geometry, friction between the bolt and hole and bolt clamp-up can only really be treated rigorously within a finite element framework and most strength prediction methods are therefore based on FEA, either two-dimensional or (in a relatively limited number of studies) three-dimensional. Chang et al., [4] carried out a number of studies on composite bolted joints and applied the concept of

* Corresponding author. Tel.: +60 7 4534472; fax: +60 7 4536588.
E-mail address: hilton@uthm.edu.my (H. Ahmad).

1359-835X/$ - see front matter © 2013 Elsevier Ltd. All rights reserved.
http://dx.doi.org/10.1016/j.compositesa.2013.10.012

the Whitney–Nuismer characteristic distances for open holes to strength prediction for a bolted joint. In formulating their model, they assumed a co-sinusoidal distribution of radial stress (from the bolt) on the inner surface of the hole and suggested that the characteristic distance (over which a failure criterion, in their case Yamada-Sun [5], has to be satisfied) varied from a critical tensile value at the location corresponding to net-tension failure to a critical compressive value at the location immediately beneath the bolt, corresponding to failure in bearing. They demonstrated reasonable agreement between the predicted and the experimental strengths and corresponding failure modes. However, there are shortcomings in such an approach, most obviously the simple treatment of the bolt-hole contact, the omission of the bolt clamp-up and the assumption that the same characteristic distances can be applied in different contexts (open hole and loaded hole) where the stress gradients are very different.

Aktas et al. [6,7] determined the failure strength and failure mode experimentally and numerically for woven-carbon and woven-glass epoxy composite pinned joints. For the modelling a two dimension finite element approach was used to determine the stress distribution in each ply and a failure criterion based upon Yamada-Sun was implemented in the ANSYS finite element code. Good agreement between numerical and experimental results for strength and failure mode of single-lap and double-lap pinned joints was obtained.

Lessard and Shokrieh [8] also developed a 2-D finite element model for a pinned joint, in their case incorporating non-linear material behaviour and geometric non-linearity. The pin-hole interaction was approximated by applying a radial boundary condition to nodes located around the hole, which is not as accurate as modelling the actual interaction between pin and hole. This was tackled more rigorously using a master–slave contact interaction by Camanho and Matthews [9] who extended a 3-D FEA model to double-lap joints, following the progressive damage model of the 2-D open hole work by Tan et al., [10]. They found that a progressive damage model consisting of stress analysis, a failure prediction and damage-dependent constitutive equations was able to simulate damage progression and accurately predict failure mode, joint stiffness and joint strength.

Karakuzu et al., [11] studied joint geometry effects in woven glass-vinyl ester composites, considering values of W/d and e/d between 2 and 5. They determined damage growth and bearing strength based on the Hashin failure criterion [12]. Although they developed a 3-D model, the bore of the hole was constrained in a radial direction to idealise the pin traction. Good agreement between measured and predicted strengths was reported. It should be noted however that this approach, as with those described already, does not capture clamp-up effects in a rigorous way, nor does it explicitly simulate the damage seen experimentally.

One way to simulate damage growth and fracture in bolted joints, specifically in the net-tension mode, is through the use of damage zone models. Hollmann [13] applied a damage zone model (DZM), developed initially for notched strength prediction by Arronsson and Backlund [14], to model the failure of graphite/epoxy composite bolted joints. The use of the DZM requires only one FEA computation of damage as compared with the ply-by-ply approach of a Progressive Damage Model (PDM), and this makes the DZM faster and easier to use when analyzing the strength of bolted joints. The framework used by Hollman was 2-D and the fracture energy was obtained by calibrating the model using experimental data for joint strengths, rather than through independent measurement. Nonetheless the approach has promise for situations where damage and fracture proceed in a self-similar manner.

A more recent approach to modelling crack growth is through the Extended Finite Element Method (XFEM) presented by Belytschko and Black [15]. In this approach local enrichment functions for the nodal displacement are used to model crack growth and separation between crack faces. Moes et al. [16] successfully simulated crack initiation and propagation along an arbitrary path without requiring either the mesh to match the geometry of the discontinuities or re-meshing near the crack. Discontinuities of the crack are simulated as enriched features by allowing discontinuities to grow through the enrichment of the degree of freedom of nearby nodes with special displacement functions. As the crack-tip changes position due to loading conditions, the XFEM algorithm creates the necessary enrichment functions for the nodal points of the finite elements around the crack tip. This approach is a very useful modelling technique because a crack in a structures can be easily tracked and the failure mode can be observed visually.

The purpose of the current work is to present an improved strength prediction methodology for woven fabric composite joints that fail by net-tension. In GFRP and CFRP woven fabric composites it has been shown that failure of notched samples tested in tension proceeds in a self-similar manner involving matrix cracking, delamination and fibre tow fracture [17,18]. In previous work [19] we showed that the notched strength of these woven fabric composites could be modelled accurately using a finite element model and a failure criterion based on the formation of a damage zone for which the input parameters (unnotched strength and toughness) could be taken from independent experiments. The net-tension failure mode in a bolted joint would be expected to be similar to that seen at an open hole and indeed we have seen that for GFRP woven fabric joints [18] the same local failure mechanisms operate.

The current paper builds on these previous works as follows. First the results of an experimental programme on the bearing strengths of woven fabric CFRP double-lap bolted joints are presented. The work includes a variety of lay-ups and the effects of joint geometry (hole size and joint width) and bolt clamp-up are investigated. This is followed by the development of a three-dimensional FEA model, which incorporates the bolt-hole interaction and frictional load transfer in a representative way. Crack propagation is simulated using XFEM with independently determined input parameters and the predictions for the bearing strength are then compared with experimental values.

Table 1
Material properties of the woven CFRP laminates* under investigation.

Laminate designation	Thickness t (mm)	E_x, E_y (GPa)	E_z (GPa)	ν_{xy}	ν_{yz}, ν_{zx}	G_{xy} (GPa)	G_{yz}, G_{zx} (GPa)	V_f (%)
PX2	0.51	50.4	11.9	0.10	0.10	4.42	3.98	44.3
PX4	1.03	51.4	11.7	0.09	0.10	4.42	3.90	43.4
5X2	0.81	45.1	12.9	0.08	0.11	3.78	3.89	38.8
5X4	1.60	47.0	12.7	0.06	0.11	3.78	3.85	38.3
PQ4	1.02	37.2	11.9	0.35	0.30	13.75	3.98	44.3
PQ8	2.03	36.8	12.1	0.33	0.30	13.86	4.04	45.0
5Q12	4.62	34.8	13.1	0.32	0.30	13.15	3.96	39.6

V_f = fibre volume fraction.
PX2 = two-layer cross-ply plain weave.
x,y = in-plane coordinates.
PX4 = four-layer cross-ply plain weave.
z = out-of-plane coordinate.
5X2 = two-layer cross-ply five harness satin weave.
t = laminate thickness.
5X4 = four-layer five harness satin weave.
PQ4 = four-layer quasi-isotropic plain weave.
PQ8 = eight-layer quasi-isotropic plain weave.
5Q12 = twelve layer quasi-isotropic five harness satin weave.
* data from Belmonte et al. [16].

Table 2
Range of test parameters investigated for CFRP DLJ tests.

Laminate	e/d	W/d	Hole size, d (mm)	Clamp-up torques (N m)
PX2	6 (fixed)	2, 3	5, 10	FT[a], 5
PX4	6 (fixed)	2, 3	5, 10	FT[a], 5
5X2	6 (fixed)	2, 3	5, 10	FT[a], 5
5X4	6 (fixed)	2, 3	5, 10	FT[a], 5
PQ4	4 (fixed)	2, 3, 4, 5	5, 10	FT[a], 5
PQ8	4 (fixed)	2, 3, 4, 5	5, 10	FT[a], 5
5Q12	4 (fixed)	2, 3, 4, 5	5, 10	FT[a], 5

[a] FT = Finger-tight.

2. Experimental study of woven CFRP bolted joints

Seven CFRP woven fabric lay-up configurations are studied in the current work. These represent a sub-set of those tested by Belmonte et al. [17] in their investigation of open-hole behaviour. Details of the lay-ups considered and some of their properties are shown in Table 1. The laminate designation and test matrix are given in Tables 1 and 2 respectively. It can be seen that configurations considered include both cross-ply and quasi-isotropic lay-ups in both plain and five harness satin weaves. The main parameters varied for each configuration are hole diameter (d), bolt loading and plate width to hole diameter ratio (W/d). Both weave types (plain weave and five harness satin weave) used Toray T300 high strength carbon fibres and were manufactured from Primco Prepregs. The epoxy resin system, which controls the matrix dominated properties such as the transverse strength, was Vantico MY750. All of these CFRP woven fabric systems were fabricated by St. Bernard Composites Ltd. CFRP panels were cut with a water-cooled diamond saw to prepare the coupons for testing. Holes of diameter 5 mm or 10 mm were introduced into each coupon using high speed steel drill bit.

The double-lap bolted joint test geometry is illustrated in Fig. 1. The CFRP plate is located centrally within the joint configuration with 3 mm thick, high yield strength ($\sigma_y = 720\ N/mm^2$) stainless steel plates, on either side. The fastener systems used in this joint configuration were steel washers and steel bolts. M5 and M10 bolts and washers were used with the 5 mm and 10 mm holes respectively. Two steel washers were provided for both bolt types, one below the bolt head and the other above the nut. The installation torques studied were a finger-tight condition (equivalent to about 0.5 N m) and a clamped condition of 5 N m. The finger-tight condition is used in composite joint design in many applications as the worst case scenario, allowing an appropriate safety factor to be determined. Since the main aim in the current work was to study net-tension failure for any given lay-up (material type and thickness), the end distance was fixed and the joint width was varied accordingly.

At least three specimens (only two specimens for the 5Q12 lay-ups with $W/d \geqslant 4$) for each joint configuration were tested to failure using an Instron test machine with a 100 kN load cell and operating at a cross-head displacement rate of 0.5 mm/min. The load–displacement response was logged and the average bearing stress at failure was recorded for each specimen. Three specimens appeared sufficient for determining the strength since most test configurations showed good (better than ± 10%) reproducibility. The measured strengths are summarised in Table 3.

There were two types of final failure mode observed in the tests, i.e. net-tension and bearing failures. Some specimens showed progressive bearing damage, likely to be associated with a combination of matrix cracking, delamination and fibre compressive failure immediately beneath the bolt, which led to repeated load drops in the load displacement response. For the joints that fail in net-tension (most of the joints), tow fractures may develop at the hole edge before ultimate failure. This has been seen experimentally in GFRP bolted joints [20], but such tow fractures, if present in CFRP, could not be observed directly.

As expected, net-tension failures displayed the lowest failure loads and failure was catastrophic. The failure load increased with increasing W/d ratio, which reflects the reduction in the stress level in the joint as the size increases. Progressive bearing failures occurred at larger W/d ratios, discussed further below. Fig. 2 shows the load–displacement curve for the tested geometries of double-lap joint having the PQ4 lay-up and 10 mm diameter hole, under both finger-tight and clamped conditions. Comparing the horizontal axes in Fig. 2(a and b), it is clear that the joint extensions at failure achieved in the finger-tight coupons are at least a factor of two larger than those achieved in the clamped joints.

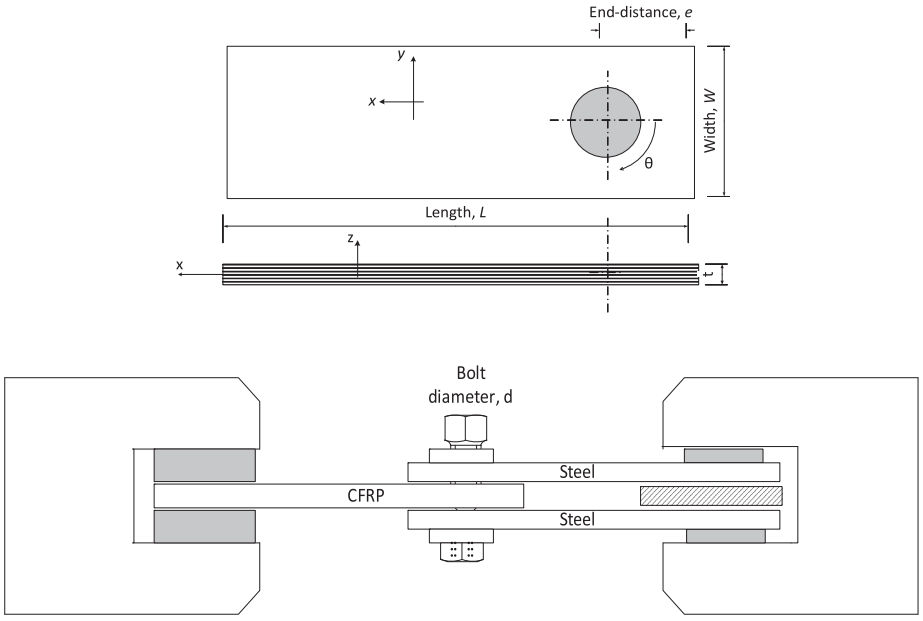

Fig. 1. Schematic of the double-lap joint configuration used in present study and CFRP plate plane view.

Table 3
Comparisons of FEA with experimental bearing strengths for woven composite CFRP double-lap joints with those predicted from 3-D FEA (note that B and NT denote bearing and Net-tension failure).

Materials	Hole diameter, d (mm)	Clamp-up torque	W/d	Experimental bearing strength (N/mm^2)	Failure mode	Bearing strength from 3D Model (N/mm^2)	% difference
PX2	5	FT	2	377 ± 15	NT	367	−2.8
			3	513 ± 39	NT	565	10.1
		5 N m	2	673 ± 41	NT	726	7.9
			3	992 ± 56	NT	978	−1.4
	10	FT	2	350 ± 42	NT	301	−13.9
			3	413 ± 40	B-NT	440	6.4
		5 N m	2	434 ± 6	NT	390	−10.3
			3	622 ± 46	NT	530	14.8
PX4	5	FT	2	388 ± 19	NT	387	0.4
			3	525 ± 32	NT	588	12.1
		5 N m	2	533 ± 21	NT	563	5.7
			3	717 ± 80	NT	773	7.8
	10	FT	2	334 ± 25	NT	312	−6.6
			3	480 ± 21	B-NT	453	−5.8
		5 N m	2	370 ± 25	NT	347	−6.4
			3	557 ± 22	NT	486	−12.7
5X2	5	FT	2	357 ± 2	NT	345	−3.3
			3	495 ± 21	NT	552	11.5
		5 N m	2	442 ± 41	NT	511	15.6
			3	664 ± 83	NT	785	18.3
	10	FT	2	275 ± 22	NT	289	5.0
			3	364 ± 13	NT	425	16.7
		5 N m	2	336 ± 19	NT	330	1.7
			3	488 ± 26	NT	466	−4.41
5X4	5	FT	2	330 ± 37	NT	308	−6.7
			3	468 ± 26	NT	511	9.2
		5 N m	2	360 ± 10	NT	474	32.0
			3	605 ± 34	NT	631	4.4
	10	FT	2	261 ± 18	NT	281	7.6
			3	435 ± 7	NT	404	−6.5
		5 N m	2	298 ± 36	NT	300	0.8
			3	441 ± 12	NT	418	−5.2
PQ4	5	FT	2	261 ± 15	NT	297	12.1
			3	457 ± 18	NT	543	18.7
			4	615 ± 28	B-NT	688	11.9
			5	698 ± 45	B-NT	796	14.0
		5 N m	2	380 ± 16	NT	437	15.0
			3	668 ± 77	NT	712	6.5
			4	847 ± 67	NT	872	3.0
			5	1005 ± 66	B-NT	972	3.2
	10	FT	2	247 ± 13	NT	287	15.9
			3	466 ± 2	NT	442	−5.3
			4	505 ± 85	B	544	7.7
			5	464 ± 9	B	613	32.1
		5 N m	2	306 ± 15	NT	311	1.7
			3	508 ± 37	NT	464	−8.4
			4	789 ± 115	NT	570	−27.8
			5	779 ± 6	B	637	−18.2
PQ8	5	FT	2	242 ± 7	NT	275	13.5
			3	454 ± 18	NT	550	21.1
			4	656 ± 25	NT	662	0.8
			5	782 ± 66	B-NT	757	−3.2
		5 N m	2	288 ± 13	NT	342	18.9
			3	536 ± 11	NT	601	12.1
			4	713 ± 19	NT	736	3.4
			5	905 ± 23	B-NT	829	−8.4
	10	FT	2	243 ± 7	NT	293	20.4
			3	434 ± 19	NT	442	1.8
			4	571 ± 25	B	526	−7.8
			5	613 ± 9	B	597	−2.7
		5 N m	2	259 ± 8	NT	294	13.2
			3	448 ± 12	NT	446	−0.6
			4	603 ± 1	NT	538	−10.8
			5	707 ± 42	B	603	−14.7
5Q12	10	FT	2	194 ± 6	NT	207	6.8
			3	364 ± 4	NT	386	6.0
			4	508 ± 34	NT	449	11.6
			5	610 ± 30	B-BT	512	16.0

(*continued on next page*)

Table 3 (*continued*)

Materials	Hole diameter, d (mm)	Clamp-up torque	W/d	Experimental bearing strength (N/mm^2)	Failure mode	Bearing strength from 3D Model (N/mm^2)	% difference
		5 N m	2	206 ± 4	NT	225	9.1
			3	372 ± 10	NT	378	1.7
			4	485 ± 27	NT	455	6.2
			5	576 ± 56	NT	505	12.3

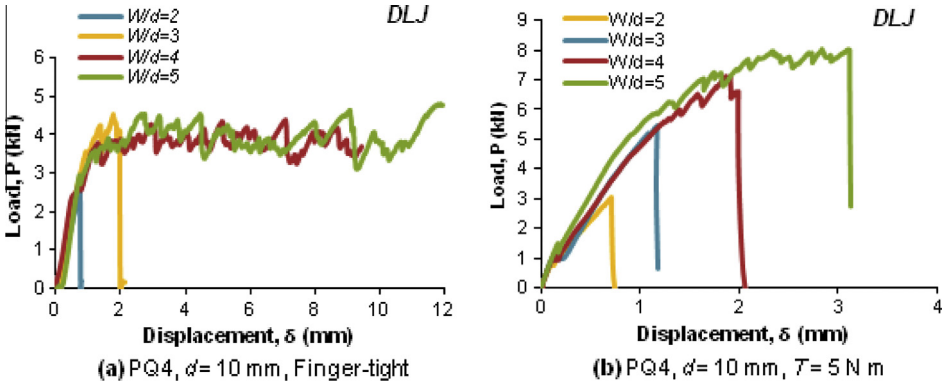

Fig. 2. Typical load–displacement curve in DLJ as a function of W/d (For interpretation of the references to colour in this figure legend, the reader is referred to the web version of this article.).

Fig. 3 shows failed coupons of four-layer plain weave quasi-isotropic lay-up, PQ4, in the clamped (T = 5 N m) condition. Net-tension failure occurred with $2 < W/d < 4$, whereas $W/d = 5$ showed a bearing mode of failure. Net-tension failures at low W/d were sudden and catastrophic. For coupons tested in the finger-tight condition, the critical W/d ratio (i.e. the value of W/d at which the failure mode changed from net-tension to bearing) was reduced to 4 and local bearing failure prior to ultimate failure was apparent in all samples. In Fig. 3 the hole elongation is obvious for the coupon with $W/d = 5$. Although difficult to see in Fig. 3, there was also evidence of local bearing damage in the coupon with $W/d = 3$. Stockdale and Matthews [21] reported a 40% increase in GFRP pin loaded bearing strength for a finger-tight case which increased to as much as 100% at their maximum clamping load (a bolt tension of 14.7 kN, which corresponds to a torque of 15 N m).

For the two cross-ply woven materials (PX and 5X) net-tension failure was observed for all the joints tested, except for the finger-tight clamped, larger hole size with $W/d = 3$. The other joints with $W/d = 3$ (10 mm hole size clamped, 5 mm hole size clamped and finger-tight) showed an initial local bearing failure, but ultimate failures was by net-tension mode; this mode of bearing failure is most apparent in the PX2 and 5X2 coupons.

The experimental strength of double-lap joints for all the CFRP woven fabric systems studied are shown in Fig. 4 and the full set of data are presented for each material in Table 3. Fig. 4(a and b) shows the data for the hole size of 5 mm in the finger tight and clamped conditions, respectively, while Fig. 4(c and d) shows the corresponding data for the hole size of 10 mm. Looking at the values of bearing strength for each hole size, it is apparent, as expected, that the torque joints generally exhibit higher values of bearing strength than their finger tight counterparts, due to the increased load transferred by friction in the former. The strength enhancement is greatest (around 50%) in the (thinnest) PX2 laminate and the extent of the increase is smaller in the other materials, with the (thickest) 5Q12 material showing a negligible increase. This is reasonable because a given frictional load will lead to a larger percentage contribution to the bearing stress as the laminate thickness decreases. Comparing the data for the two cross-ply lay-ups, the plain weave fabric systems (PX2, PX4) show bolted joint strengths that are greater (by 5–40%) than those for the corresponding five-harness satin fabric systems (5X2, 5X4). Similar trends were also observed by Belmonte [17] for open-hole strength and are likely to be a consequence of the higher fibre volume fraction of plain weave (44% compared to 39% – see Table 1), even though plain weave exhibits a higher degree of crimp as compared to equivalent five-harness satin fabric. The higher fibre volume fraction in the plain weave fabric is attributed to the ability of the fabric to nest the fibres more tightly than the five harness satin. Comparing the data for the different hole sizes (Fig. 4(a and c) for

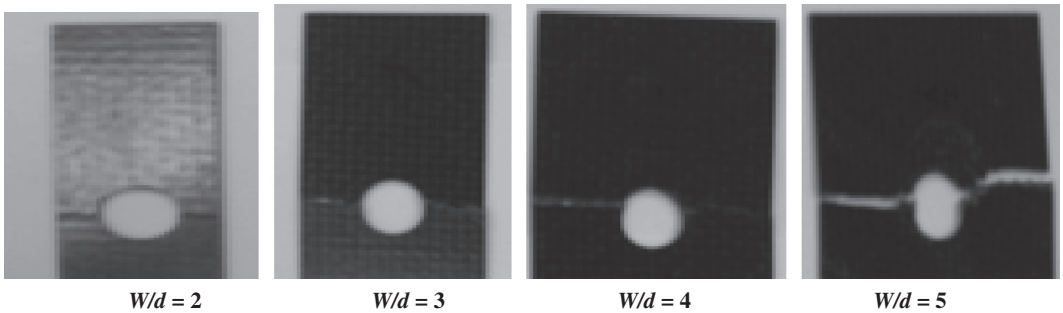

Fig. 3. Plan view photographs of failed double-lap joint (DLJ) specimens with varying normalised joint width, W/d – material type PQ4 and joints were tested in the clamped condition.

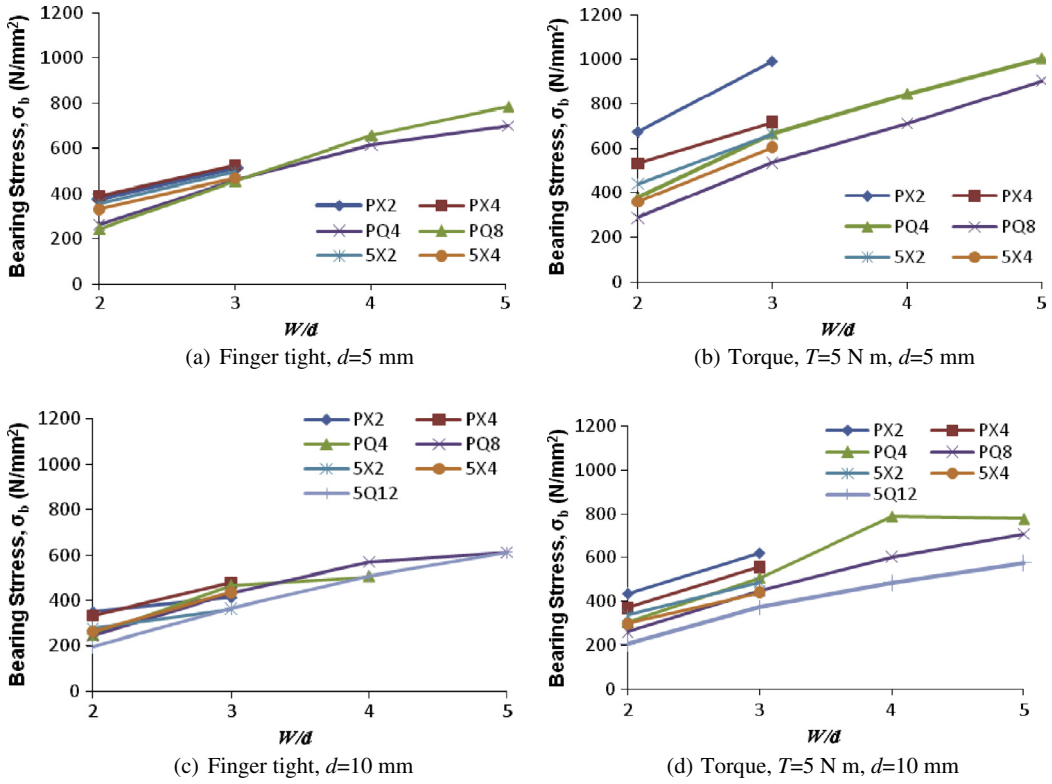

Fig. 4. Bearing stress at failure as a function of normalised joint width, W/d, for the range of woven fabric laminates tested. Fig. 4(a and b) show results for the 5 mm diameter holes in the finger tight and clamped conditions, respectively, while Fig. 4(c and d) show the corresponding results for the 10 mm diameter holes (For interpretation of the references to colour in this figure legend, the reader is referred to the web version of this article.).

the two hole sizes in the finger-tight condition, Fig. 4(b and d) for the two hole sizes in the clamped condition), it can be seen that at a given W/d ratio there is a reduction in the bearing stress at failure in the joints with a hole size of 10 mm compared to those with a hole size of 5 mm, the reduction varying from around 10% to 40% depending on the laminate lay-up and thickness. The stress concentration effect is independent of the hole diameter at a constant W/d and so this reduced strength represents a 'hole size' effect although a reduced frictional load transfer at larger d/t ratio may be a contributory factor.

3. Finite element modelling of woven CFRP bolted joints

3.1. Bolted joint geometry and material properties

3-D models are able to include friction load transfer explicitly, leading to a more representative simulation than is possible with a 2-D model. Elastic properties of the woven fabric composites used in the model are based on smeared-out in-plane and out-of-plane properties, see Table 1. All joint parts are assembled by defining the interaction (with appropriate friction values) between all contacting surfaces. Boundary conditions and applied loading are assigned to appropriate surfaces and edges to simulate the mechanical testing of the bolted joint configurations. Due to symmetry, only half of the configuration is modelled, thus saving computational costs and efforts.

The bolted joint systems in the test matrix have varying dimensions. All joints have a fixed e/d ratio but their W/d and/or d/t ratios, and bolt loading will change. Although these variations may change the composite failure mechanisms, the main aim is to predict the failure that is exhibited through net-tension mode. In the double-lap joint, seven separate parts are assembled; the composite plate is sandwiched between two steel plates and fastened with a single steel bolt. The washers and bolt are modelled separately to represent the real load transfer due to friction.

A typical mesh of a joint model is shown in Fig. 5. Symmetry about the joint mid-plane is modelled in all cases for computational efficiency. The mesh was refined in the vicinity of the hole (under the washers), while away from the hole, the mesh was made coarser. The number of degrees of freedom for these bolted joint models is about 100,000. Eight-node linear brick elements (C3D8 in ABAQUS [22]) are used because these elements are compatible with the XFEM-based failure model. Boundary conditions were assigned to provide realistic loading. The end faces of the steel plates are restrained in all degrees of freedom at one end of the model [A in Fig. 5], while an axial displacement is applied to the composite plate end face at the other end of the model [B in Fig. 5].

The effect of bolt tension and the subsequent loading of the joint are treated as two loading steps in the current work. This is illustrated in Fig. 6. The first step consists of applying the bolt load to the joint and in the second step, the far-field tensile load on the steel and composite plates is applied. Within the FE model, the lateral clamping force (the bolt tension) remains constant throughout the second step. This modelling work implemented large displacement analysis (non-linear geometry) to best capture the contact interactions. The amount of bolt load depends upon the clamp-up torque used (either finger-tight (0.5 N m) or a torque of 5 N m). Friction load is determined from the experimental results and preload were determined using an assumed static friction coefficient of 0.3, the average load in the bolt associated with CFRP tests was found to be 1250 N when a torque of 5 N m was applied to the bolt and 125 N when a finger-tight load was used.

A perfect fit between the bolt and the hole was assumed. Master–slave contact interactions were applied between the regions in contact. A total of eleven master–slave interactions were assigned

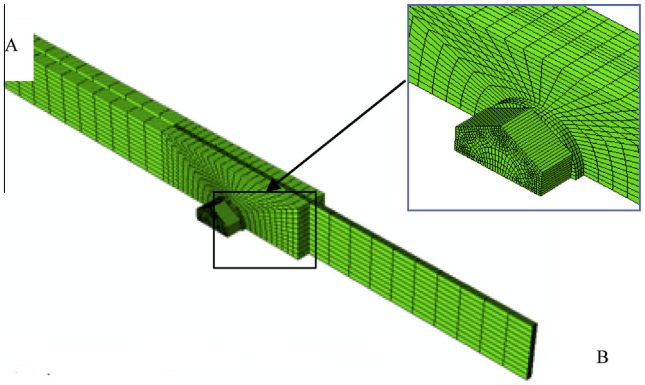

Fig. 5. Finite element model of double-lap bolted joint implemented in ABAQUS CAE. (For interpretation of the references to colour in this figure legend, the reader is referred to the web version of this article.)

between corresponding contact pair faces. Meshing on the master surface is coarser than on the slave surface, following best practice. Friction coefficients are assigned to the contact region in the model. Coefficients of friction of 0.1 for steel-steel (plate-fastener) and 0.3 for the composite-steel (overlap region) were used (these values are similar to those used by other researchers, e.g., McCarthy et al. [23]). The procedure used to model the bolt load was suggested by ABAQUS CAE [22], whereby the bolt is pre-tensioned prior to the application of the far-field tensile load. Stresses generated in the bolt shaft were viewed and found to correspond to the pre-load applied.

3.2. Implementation of constitutive damage law in FE modelling

The crack initiation and propagation found in open-hole problems is similar to net-tension failures found in bolted joint problems, enabling similar approaches to be used in both. The failure model used for net-tension involves the bi-linear traction–separation relationship shown in Fig. 7, implemented within an XFEM region [22]. Damage initiation and propagation from the hole edge was modelled and was consistent with the failure pattern within the damage zone that were observed experimentally. The maximum stress, σ_o and critical fracture toughness values of the CFRP laminates, G_c used in the bi-linear traction–separation relationship are given in Table 4 taken from Belmonte et al. [17]. It is important to note that as for the open-hole problem, σ_o and G_c were taken from independently measured un-notched strength and toughness of woven composite lay-up plates and were not calibrated to fit the measured double lap bolted joint data.

In the present work, the crack domain was assigned to a region in the model around the hole edge from where the crack is observed to initiate. The remainder of the composite plate was assigned as the un-cracked domain. This description is illustrated in Fig. 8. Damage propagation has been simulated using the Extended Finite Element Method (XFEM). The XFEM formulation is embedded in ABAQUS CAE [22] which is based on the integration of an enriched function with additional degrees of freedom but retaining properties such as sparsity and symmetry of the stiffness matrix. This enriched function consists of near-tip asymptotic functions to capture the singularity around the crack-tip and a discontinuity function that allows modelling of the displacement jump between crack faces during crack propagation.

ABAQUS initiates and propagates damage at regions experiencing principal stresses greater than the corresponding limiting values (critical traction) specified in traction–separation law. Crack initiation and crack propagation will always take place orthogonally to the maximum principal stresses. The strength prediction is relatively mesh independent since crack growth is controlled by the fracture energy (G_c). It should be emphasised that, due to the intrinsic principles of XFEM, only one strength parameter triggering the damage initiation was introduced in ABAQUS [22], the maximum principal stress. Damage evolution is controlled by a damage parameter, d_i, which is determined from the current separation, and the release separation (determined from G_c and σ_o). Fracture makes the structural response non-linear and numerical methods can experience difficulty converging to a solution. A damage stabilisation coefficient has been used to facilitate

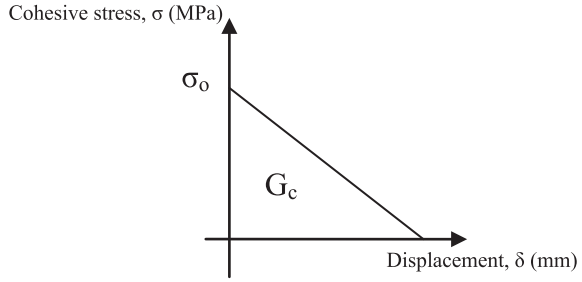

Fig. 7. Assumed traction–displacement response for the physically-based constitutive model used in the current analysis.

Table 4
Maximum traction and toughness values used in current model, data from [16].

Material	σ_o (MPa)	G_{IC} (kJ/m^2)
PX2	481	26.0
PX4	527	27.7
5X2	419	28.8
5X4	535	20.0
PQ4	390	21.6
PQ8	428	17.9
5Q12	370	12.9

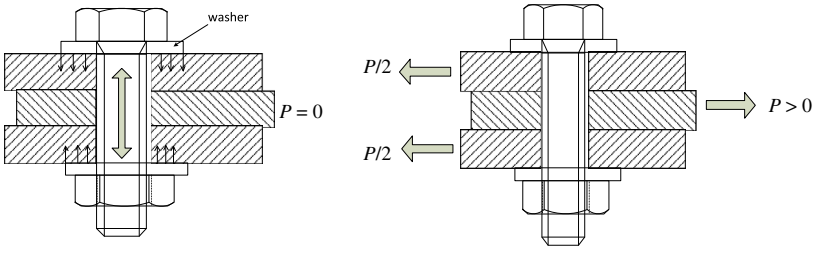

(a) Pre-load (b) Far-field applied load

Fig. 6. Two loading steps implemented in finite element modelling of clamped joints (a) Pre-load and (b) Application of in-plane load (For interpretation of the references to colour in this figure legend, the reader is referred to the web version of this article.).

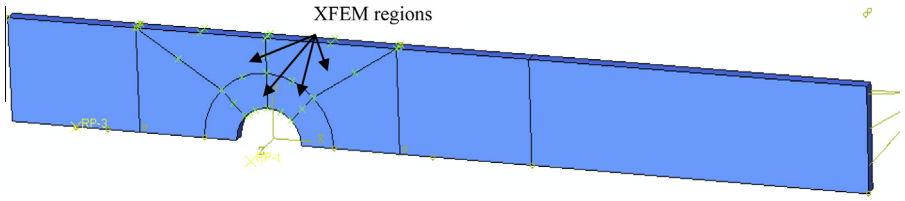

Fig. 8. Regions assigned for XFEM modelling in the present work (For interpretation of the references to colour in this figure legend, the reader is referred to the web version of this article.).

convergence. This stabilisation takes the form of viscous damping, adding forces where sudden damage occurs. A parametric study was undertaken to determine the optimum value (small enough not to influence the solution values but large enough to allow convergence to be obtained). This is discussed further in Section 4.

4. Stress distribution and strength prediction

Two different lay-ups of similar thickness (PX4 and PQ4) are compared giving the stress profiles shown in Fig. 9. Fig. 9 shows three different stress distributions, the radial stress immediately below the bolt (9a), the tangential stress around the hole boundary (9b) and the longitudinal stress on the net tension plane (9c). For each part of the figure the results are shown for the PQ4 and PX4 laminates in both the finger tight and clamped conditions for an applied bearing stress of 400 N/mm^2. The different lay-ups give different tangential stress distributions along the hole boundary. The quasi-isotropic laminate has ± 45° plies and exhibits a single peak in the tangential stress, which increases from around 100 N/mm^2 at the bearing plane to peak at around 600 N/mm^2 at about 85° and decreases subsequently. The stress peaks occurred at the end of contact regions. Cross-ply lay-ups have no ±45° plies and showed a minimum tangential stress at an angle of 45° from bearing plane. Additionally, two peaks are produced at 0° and 90° associated with $(0/90)_{ns}$ lay-up where the second tensile stress peak was around twice than the first peak and occurred at a location where the bolt-hole contact ended. These trends are a consequence of the local changes in lay-up geometry around the hole boundary in a polar co-ordinate system. The tensile stress at the net-tension plane of 1000 N/mm^2 in the cross-ply lay-up compared to a value of 600 N/mm^2 for the quasi-isotropic lay-up is a consequence of the anisotropy of the cross-ply. In contrast, both lay-ups showed a similar distribution in the radial stress distribution. Similar trends were obtained by Crews et al. [24] who studied the stresses using a 2-D model for a bolted joint with six different (non-woven) laminate lay-ups and found that there was strong influence of anisotropy in magnitude and location of peak tangential stress.

Two studies have been carried out to determine the appropriate mesh size and the appropriate coefficient of damage stabilization. This part of the study was conducted using the PQ4 lay-up with hole diameter of 5 mm with $W/d = 3$ and in a clamped condition. Different mesh sizes have been considered in the vicinity of the hole because this is the region of interest (failure). As shown in Fig. 10, there is no apparent effect of mesh size on strength prediction; this finding is expected as XFEM is driven by an energetic approach, which is much less sensitive to mesh size than stress is.

Damage stabilisation studies have also been conducted to determine the most appropriate coefficient to use. A large damage stabilisation coefficient may achieve convergence more rapidly but may produce non-physically meaningful behaviour, over-predicting the bearing stress at failure as shown in Fig. 11. Nevertheless, too small a coefficient of damage stabilisation may produce convergence difficulties. From the plot in Fig. 11, a coefficient of 1×10^{-5} was sufficient to achieve convergence, without affecting the predicted strengths.

A typical predicted finger-tight clamped double-lap bolted joint load–displacement curve, specifically for a PX4 laminate with a hole size of 5 mm and $W/d = 3$, is shown in Fig. 12. Fig. 13 shows the corresponding damage evolution in the form of plots of von Mises stress (S Mises) at the locations (a–d) on the load–displacement curve in Fig. 12. Crack initiation is exhibited as shown in Point a; at this point the plate is still able to carry more load until ultimate failure as given by Point b. Point b is the maximum failure load (predicted joint strength) from current modelling work. Beyond point b, the joint will exhibit catastrophic behaviour due to the inability of the plate to carry more load, as -given in Point c and Point d. Note that because the stress distribution is modelled as uniform through the thickness of composite laminate, crack initiation and propagation events occur uniformly across the laminate. Overall Fig. 12 exhibits a similar response to that found for the open-hole problem [19]. The maximum failure load from FEA modelling of all lay-up systems is compared with experimentally measured strengths in the next paragraph.

Strength predictions of the CFRP double-lap joints using 3-D FEA modelling are compared with the experimental data in Table 3. The trends shown by these experimental data have been discussed previously in Section 2; in the present section we consider the ability of the model to capture these effects. In general, it can be observed that a discrepancy of less than 20% is obtained for most of the joint configurations with an average discrepancy of only 10%. It should again be stressed that the failure parameters used in this modelling work were not calibrated to fit the measured data but were obtained from totally independent tests, thus further establishing the efficacy of this modelling approach. There was no significant difference obtained between the various lay-ups considered. Looking at the data carefully and comparing PX2 with PX4, 5X2 with 5X4 and PQ4 with PQ8 there appears to be a trend of more accurate predictions with increasing laminate thickness. This may, in part, be because smeared-out properties are a better representation for thicker sections in woven fabric. Note also that the model correctly captures the hole size effect for bolted joints in the same-way as for open-hole specimens.

Experimentally, specimens with low W/d ratios displayed net-tension failure while bearing failure occurred at higher W/d values. Clearly, models for joints showing net-tension failures will be more reliable than for those that showed bearing failure as this mode is not accommodated in the FEA modelling. Bearing failures are due to compression behind the bolt, resulting in fibre kinking, delamination and matrix cracking, which are not represented in the currently implemented constitutive model. This behaviour is exhibited when $W/d \geqslant 3$ (finger-tight, cross-ply lay-up), $W/d \geqslant 4$ (finger-tight, quasi-isotropic lay-up) and $W/d \geqslant 5$ (all bolt loads, quasi-isotropic lay-up). For some of these geometries there was a large discrepancy between the predictions and experiment, e.g. for the PQ4 laminate with a hole size of 10 mm in the finger-tight condition with $W/d = 5$ where the model over-predicted by 32%, but for others, e.g. for the PQ4 laminate with a hole size of

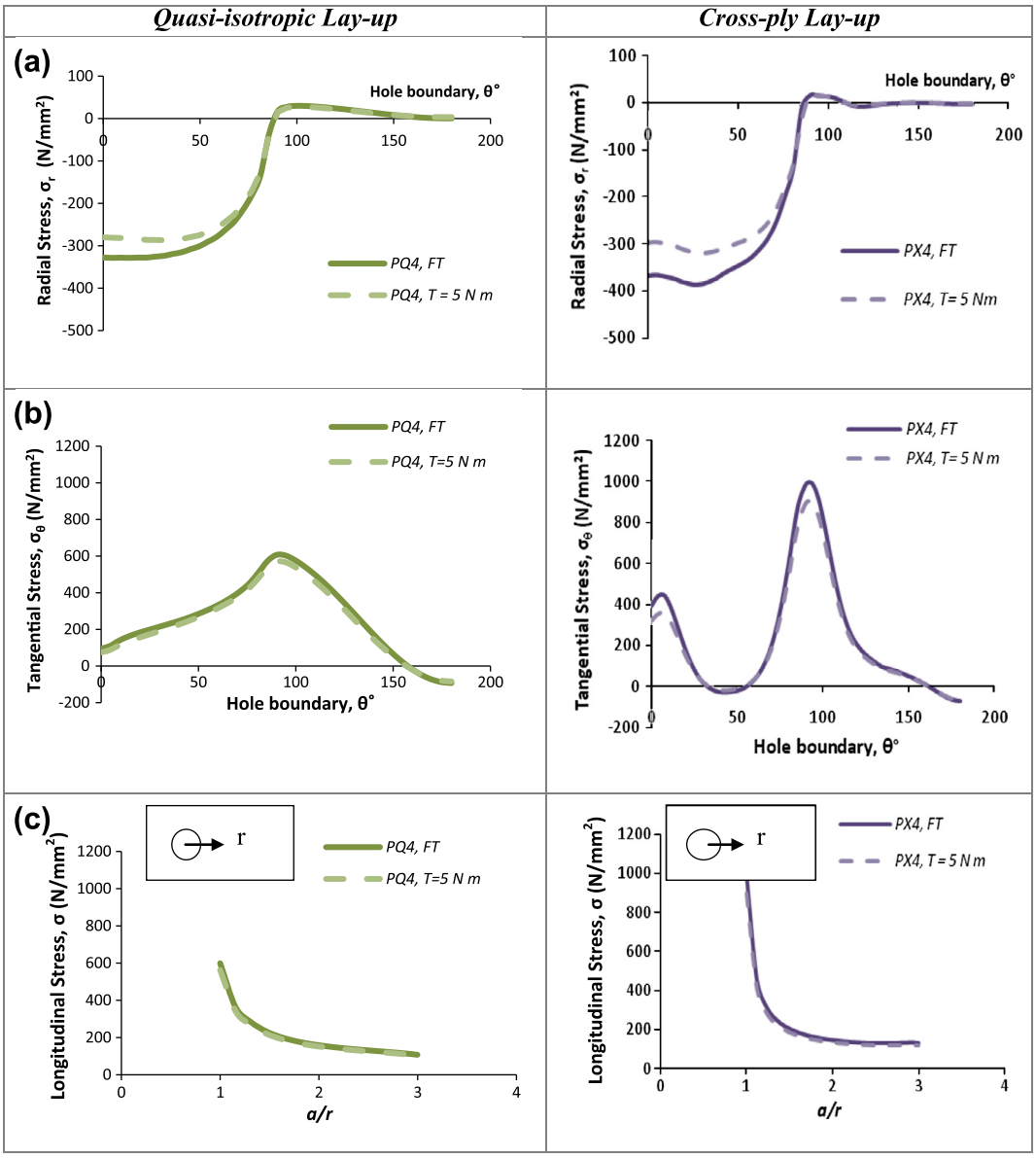

Fig. 9. Comparison of FEA stress distributions near loaded hole in quasi-isotropic (PQ4) and cross-ply (PX4) lay-ups with $d = 10$ mm in the finger-tight and clamped conditions at an applied bearing stress of 400 N/mm^2 (a) Radial stress around hole boundary (b) Tangential stress around hole boundary and (c) Longitudinal stress with normalised distance from the hole edge (For interpretation of the references to colour in this figure legend, the reader is referred to the web version of this article.).

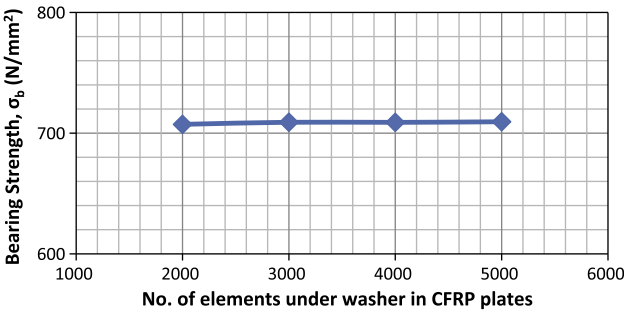

Fig. 10. Results from parametric study to explore any mesh sensitivity effect on predicted bearing strength for a clamped double-lap woven CFRP composite joint (PQ4, hole size 5 mm, $W/d = 3$) in the clamped condition (For interpretation of the references to colour in this figure legend, the reader is referred to the web version of this article.).

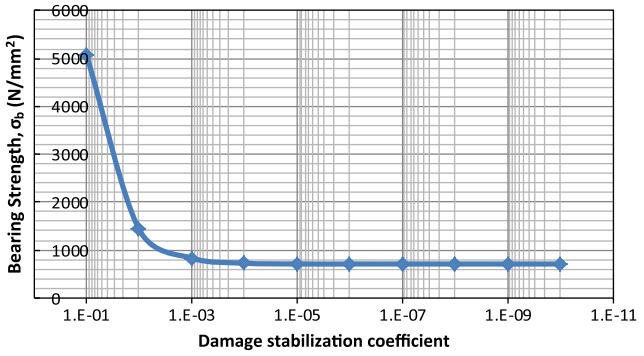

Fig. 11. Results from parametric study to explore the effect of varying the damage stabilization coefficient on predicted bearing strength for a double-lap woven CFRP composite joint (PQ4, hole size 5 mm, $W/d = 3$) in the clamped condition (For interpretation of the references to colour in this figure legend, the reader is referred to the web version of this article.).

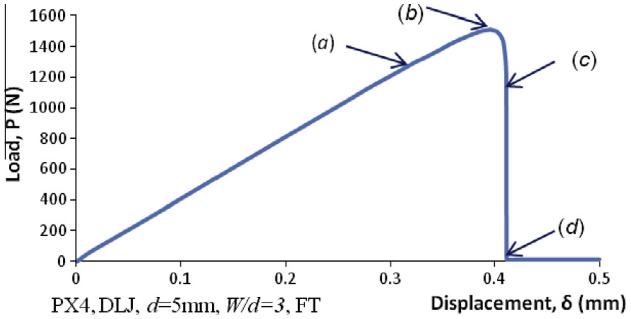

Fig. 12. Typical load–displacement curve for double-lap joint from 3-D FEA – results shown were obtained for a double-lap woven CFRP composite joint (PX4, hole size 5 mm, $W/d = 3$) in the finger-tight condition. (For interpretation of the references to colour in this figure legend, the reader is referred to the web version of this article.)

10 mm in the finger-tight condition with $W/d = 5$, agreement remained reasonable (within 3%). Additional work is needed to explore these issues in more detail. The predicted load–displacement plots showed the same trend in all bolted double-lap joints studied. The length of damage zone/effective crack at the point of sudden failure is in the range of 0.4–0.8 mm from the hole edge at the net-section plane.

5. Concluding remarks

An extensive range of woven fabric CFRP – steel bolted double lap joints have been manufactured and tested to determine their joint strengths. Parameters considered included composite architecture lay-up, bolt load and plate width to hole diameter ratio W/d and bolt clamp-up. Three dimensional finite element modelling has been undertaken on the specimens tested experimentally. The bolt load and the associated friction have been included explicitly in this modelling work. Strength predictions are obtained using a traction–separation damage model based on the Extended Finite Element Method (XFEM). The damage modelling approach in these bolted double-lap joints is similar to that used in the open-hole problem [19], as the failure mode resembles the open-hole failure mechanism. The failure parameters used in this work are the same as those used in the open hole work and, further, these were obtained from independent materials characterisation tests and are not calibrated to fit the open hole and bolted joint results. Good agreement between predicted and experimental strengths is found, with the average discrepancy being 9.6% and most CFRP lay-ups showing a discrepancy of less than ±20%. The approach is not applicable to the situation where the dominant mode of failure is in bearing. This approach is physically-based, has been shown to be applicable to woven fabric composite materials in double-lap bolted joint, and is recommended as a means of assessing various potential bolted joint configurations.

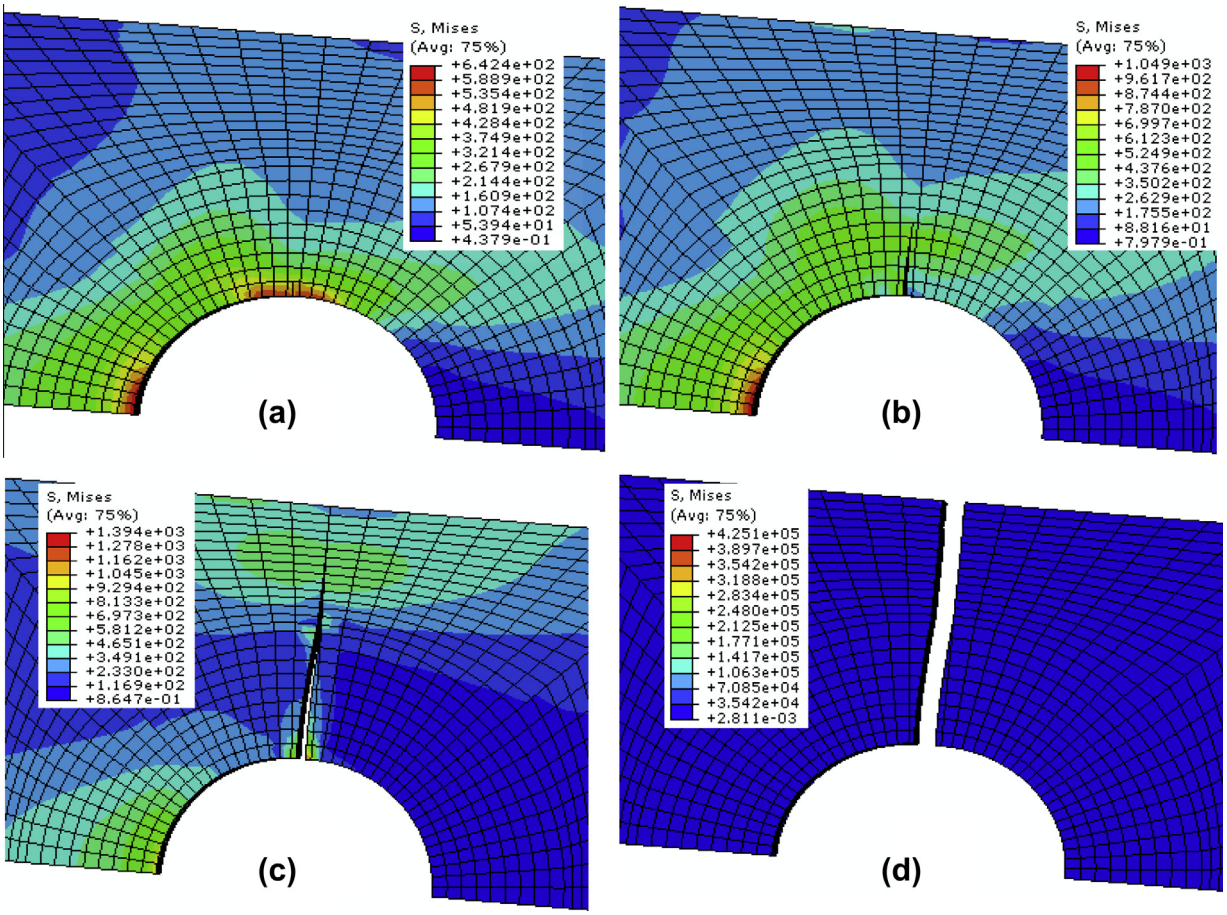

Fig. 13. Maps of von-Mises stress showing the crack growth at the four points (a–d) marked on the load–displacement curve in Fig. 12 for a double-lap woven CFRP composite joint (PX4, hole size 5 mm, $W/d = 3$) in the finger-tight condition (For interpretation of the references to colour in this figure legend, the reader is referred to the web version of this article.).

References

[1] Collings TA. The strength of bolted joints in multi-directional CFRP laminates. Composites 1977:43–55.
[2] Godwin EW, Matthews FL. A review of the strength of joints in fibre reinforced plastics – mechanically-fastened joints. Composites 1980;11:150–60.
[3] Thoppul SD, Finegan J, Gibson RF. Mechanics of mechanically fastened joints in polymer–matrix composite structures – a review. Compos Sci Technol 2009;69:301–29.
[4] Chang FK, Scott RA, Springer GS. Strength of mechanically fastened composite joints. J Compos Mater 1982;16:470–94.
[5] Yamada SE, Sun CT. Analysis of laminate strength and its distribution. J Compos Mater 1978;12:275–84.
[6] Aktas A, Dirikolu MH. An experimental and numerical investigation of strength characteristics of carbon-epoxy pinned-joint plates. Compos Sci Technol 2004;64:1605–11.
[7] Aktas A, Imrek H, Cunedioğlu Y. Experimental and numerical failure analysis of pinned-joints in composite materials. Compos Struct 2009;89:459–66.
[8] Lessard LB, Shokrieh MM. Two-dimensional modelling of composite pinned-joint failure. J Compos Mater 1995;29:671–97.
[9] Camanho PP, Matthews FL. A progressive damage model for mechanically fastened joints in composite laminates. J Compos Mater 2000; 33(24):2248–80.
[10] Tan SC. A progressive failure model for composite laminates containing openings. J Compos Mater 1991;25:556–77.
[11] Karakuzu R, Gulem T, İcten BM. Failure analysis of woven laminated glass-vinylester composites with pin-loaded hole. Compos Struct 2006;72:27–32.
[12] Hashin Z. Failure criteria for unidirectional fibre composites. J Appl Mech 1980;47:329–34.
[13] Hollmann K. Failure analysis of bolted composite joints in-plane failure modes. J Compos Mater 1996;30(3):358–83.
[14] Aronsson CG, Backlund JA. Sensitivity analysis of the damage zone model. Comput Struct 1986;22:669–76.
[15] Belytschko T, Black T. Elastic crack growth in finite elements with minimal remeshing. Int J Numer Methods Eng 1999;45:601–20.
[16] Moes N, Dolbow J, Belytschko T. A finite element method for crack growth without remeshing. Int J Numer Methods Eng 1999;46:131–50.
[17] Belmonte HMS, Ogin SL, Smith PA, Lewin R. A physically-based model for the notched strength of woven quasi-isotropic CFRP laminates. Composite Part A 2004;35:763–78.
[18] Belmonte HMS, Manger CIC, Ogin SL, Smith PA, Lewin R. Characterisation and modeling of the notched tensile fracture of woven quasi-isotropic GFRP laminates. Compos Sci Technol 2001;61:585–97.
[19] Ahmad H, Crocombe AD, Smith PA. physically based finite element strength prediction in notched woven laminates under quasi-static loading. Plast, Rubber Compos 2013;42(3):93–100.
[20] Ahmad H, Crocombe AD, Smith PA. Failure modelling of woven GFRP bolted joints under quasi-static loading. In: 18th International Conference on Composite Materials (ICCM18), Jeju Island, South Korea; 2011.
[21] Stockdale JH, Matthews FL. The effect of clamping pressure on bolt bearing loads in glass fibre reinforced plastics. Composites 1976:34–9.
[22] Dassault Systèmes Simulia Corp., Abaqus Analysis User's Manual, Version Abaqus 6.10.1, Providence, RI, USA; 2010.
[23] McCarthy MA, McCarthy CT, Lawlor VP, Stanley WF. Three-dimensional finite element analysis of single-bolt, single-lap composite bolted joints: Part I – model development and validation. Compos Struct 2005;71:140–58.
[24] Crews JH, Hong CS, Raju IS, Stress concentration factors for finite orthotropic laminates with a pin-loaded hole. 1-40, NASA Technology Paper 1862; 1981.